EURODINAME III - An International Symposium on Dynamic Problems of Mechanics
June 8-11, 2026 - Giens Peninsula, FR

EURODINAME-2026-13698
A NOVEL STRATEGY FOR INTERFACE MODEL REDUCTION EXPLORING COMPONENT-LEVEL GLOBAL MODES FOR SUBSTRUCTURING APPLICATIONS

Vinícius Mauro de Souza Santos
Aeronautics Institute of Technology, Praça Marechal Eduardo Gomes, 50 – São José dos Campos, 12228-900, SP, Brazil
Université Marie et Louis Pasteur, SUPMICROTECH, CNRS, Institut FEMTO-ST, Besançon, F-25000, France
vinicius.santos@ga.ita.br, vinicius.mauro@femto-st.fr

Thiago de Paula Sales
Aeronautics Institute of Technology, Praça Marechal Eduardo Gomes, 50 – São José dos Campos, 12228-900, SP, Brazil
tpsales@ita.br, thiago.sales@gp.ita.br

Morvan Ouisse
Université Marie et Louis Pasteur, SUPMICROTECH, CNRS, Institut FEMTO-ST, Besançon, F-25000, France
morvan.ouisse@femto-st.fr

Abstract. *Substructuring techniques are important in both industry and academia for the dynamic analysis of complex assemblies consisting of multiple components. These methods rely on coupling reduced-order models where interior degrees of freedom (DoFs) are typically reduced via the Hurty/Craig–Bampton method. However, interface DoFs often remain unreduced, leading to computational inefficiencies in models with many substructures or fine meshes. This research introduces a novel local-level model-order reduction approach designed to reduce these interface DoFs. Inspired by boundary reduction techniques devised for periodic-like structures, the proposed method calculates interface modes within a global setting that considers the coupling between a component's boundaries and its interior. To guarantee compatibility between adjacent parts, interface modes from different substructures are unified into a single, shared projection matrix. To enhance numerical stability and reduce the model size, a Modal Assurance Criterion strategy is proposed to eliminate redundant, collinear eigenvectors. Testing on a W-bracket model confirms that the novel interface reduction strategy competes with current state-of-the-art methods, delivering high accuracy.*

Keywords: *substructuring, model-order reduction, interface reduction, Hurty/Craig–Bampton, modal assurance criterion.*

1. INTRODUCTION

In the current engineering practice, computational simulation has become the norm. Whilst experiments are still required for verification of models, and to improve the human understanding of physical phenomena, most design procedures leverage simulations in one or another form. As computational power has grown since the invention of digital computers, models used in simulations have also seen an increase in their size, specially when one considers finite element models developed to capture detailed geometric features relevant for simulations, or necessitating fine spatial resolution due to time/frequency content related to required analyses.

It so happens that, while intensive simulations might be suitably tackled by supercomputers, during design, it is very much favorable to work with models of reduced size that still satisfactorily represent phenomena of interest. This is mainly on account of the iterative nature of design, i.e., one wants to conduct fast simulations to assess responses quickly, and implement modifications until design criteria are met. Even if optimization is used in such process, instead of trial-and-error, benefits provided by being able to perform low-cost simulations that still grant accurate results should be evident.

In the particular context of structural assemblies, the computation of dynamic responses has been definitely improved by means of substructuring techniques, such as component mode synthesis (CMS) strategies. These leverage dynamical features deemed relevant of components to approximately model subassemblies or an entire assembly, which might be

This work is licensed under a Creative Commons "Attribution 4.0 International" license.

complex, requiring significant simulation time otherwise.

While CMS already involves established procedures, having been developed and applied for decades, more recent research has been devoted to its improvement by considering the reduction of degrees of freedom (DoFs) related to boundaries/interfaces between components. Such reduction usually takes place in the context of the Hurty/Craig–Bampton (HCB) method — being it used to reduce interior DoFs of a substructure using fixed-interface normal modes, while accounting for interface constraint modes that allow for adequate representation of its static response.

The reduction of boundary DoFs can be performed through various strategies, including system-level characteristic constraint (S-CC) (Castanier *et al.*, 2001), exact-compatibility local-level CC (EC L-CC) (Hong *et al.*, 2013), weak-compatibility L-CC (WC L-CC) (Hong *et al.*, 2013; Kuether *et al.*, 2017; Krattiger *et al.*, 2019), uncoupled WC L-CC (Hong *et al.*, 2013; Kuether *et al.*, 2017; Krattiger *et al.*, 2019), virtual node (Lindberg *et al.*, 2013; Krattiger *et al.*, 2019), hybrid-level CC (Aoyama and Yagawa, 2001; Krattiger *et al.*, 2019) methods. Basically, these interface reduction techniques operate i) on the assembled system-level matrices, in which the substructures are coupled to each other after reducing the internal DoFs, ii) at the local-level, where interface reduction is performed on individual substructures independently, before assembly, or iii) somewhere in between the previous approaches, where connections related to a particular interface need to be considered during its reduction.

Castanier *et al.* (2001), for example, introduced the reduction of interface DoFs through a secondary eigenanalysis of the system-level stiffness and mass matrices (S-CC). Hong *et al.* (2013) improved the S-CC method by considering the reduction of interface DoFs at the substructure-level (L-CC). Tran (2001) addressed the reduction of interface DoFs in CMS methods by employing a truncated basis of interface modes. Tran (2009) derived CMS methods for interface reduction using partial interface modes that allow some DoFs to be retained during a second-level model-order reduction (MOR). Donders *et al.* (2010) proposed a wave-based substructuring scheme that reduces the interface DoFs of substructures using a limited set of basis functions computed from a single modal analysis of the full assembly model. Kuether *et al.* (2017) addressed the substructuring of geometrically nonlinear finite element models, including the reduction of internal and interface DoFs. More recently, Young and Wixom (2026) developed an interface reduction strategy for non-smooth line-line interfaces using polynomials, which also enabled the analysis of substructures with incompatible meshes.

Considering the previous context, the objective of this paper is to propose and analyze a novel strategy to perform the reduction of boundary/interface DoFs in CMS. This strategy has close relationship to, and has been motivated by work done by the authors related to periodic structures (Santos *et al.*, 2025).

To perform assessments, one considers throughout this paper the assembly illustrated in Fig. 1, analogous to one analyzed by Krattiger *et al.* (2019). The assembly contains five substructures, Ω_s, $s = 1, \ldots, 5$, modeled using SHELL181 plate finite elements; and three interfaces $\Gamma_i^{(g)}$, $i = 1, 2, 3$, their definition being shown in Fig. 1. All elements have edge sizes equal to 0.5 in = 12.7 mm. Overall dimensions are given by 12 in (304.8 mm) × 24 in (609.6 mm) × 8 in (203.2 mm) along x, y, z (Craig and Bampton, 1968; Krattiger *et al.*, 2019). Other relevant properties are presented later.

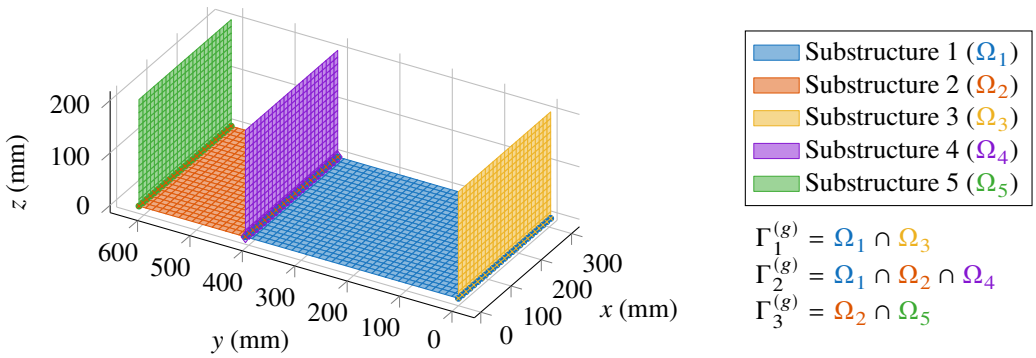


Figure 1: Finite element meshes of substructures making the assembly considered here. Nodes at interfaces are indicated using markers. All other nodes, at vertices of quadrilateral plate elements, pertain to the interior domain of substructures.

In the following, the paper presents theory related to CMS and to the reduction of interface DoFs (Section 2); aspects concerning the numerical experiments that have been run, as well as results and their discussion (Section 3); and concluding remarks (Section 4). Acknowledgments and the list of cited references are also provided afterward.

2. THEORY

In this section, a brief overview of the theory underlying this work is presented. By no means the provided explanation is self-contained, due to space limitation. Relevant works of the literature can be consulted for more in-depth details, nevertheless (Craig and Kurdila, 2006; Krattiger *et al.*, 2019; Allen *et al.*, 2020). Initially, in Section 2.1, aspects concerning the HCB method are reviewed. Afterward, in Section 2.2, one briefly discusses established techniques that have been used for reducing boundary DoFs of substructure models; and presents the alternative strategy proposed inhere.

2.1 Hurty/Craig–Bampton method

Consider a component s of a structural assembly that has been modeled by the finite element method, being it characterized by inertia and stiffness matrices $\mathbf{M}^{(s)}$ and $\mathbf{K}^{(s)}$. Its vector of generalized DoFs $\mathbf{u}^{(s)}$ can be partitioned considering it shares interfaces with other components, or which are related to boundary conditions; and the remaining interior region (cf. Fig. 1). That is to say, $\mathbf{u}^{(s)}$ can be partitioned into boundary (b) and internal (i) DoFs. The equations of motion (EoMs) then read:

$$\mathbf{M}^{(s)}\ddot{\mathbf{u}}^{(s)}(t) + \mathbf{K}^{(s)}\mathbf{u}^{(s)}(t) = \mathbf{f}^{(s)}(t) \qquad \Leftrightarrow \qquad \begin{bmatrix} \mathbf{M}_{bb}^{(s)} & \mathbf{M}_{bi}^{(s)} \\ \mathbf{M}_{ib}^{(s)} & \mathbf{M}_{ii}^{(s)} \end{bmatrix} \begin{Bmatrix} \ddot{\mathbf{u}}_b^{(s)}(t) \\ \ddot{\mathbf{u}}_i^{(s)}(t) \end{Bmatrix} + \begin{bmatrix} \mathbf{K}_{bb}^{(s)} & \mathbf{K}_{bi}^{(s)} \\ \mathbf{K}_{ib}^{(s)} & \mathbf{K}_{ii}^{(s)} \end{bmatrix} \begin{Bmatrix} \mathbf{u}_b^{(s)}(t) \\ \mathbf{u}_i^{(s)}(t) \end{Bmatrix} = \begin{Bmatrix} \mathbf{f}_b^{(s)}(t) \\ \mathbf{f}_i^{(s)}(t) \end{Bmatrix}, \quad (1)$$

where $\mathbf{f}^{(s)}$ is the vector of externally-applied loads, t denotes time, and $\ddot{\mathbf{u}}^{(s)}$ represent second-order time derivatives of $\mathbf{u}^{(s)}$. Notice time-dependencies are omitted from here onward.

In the HCB method, $\mathbf{u}_i^{(s)}$ is replaced by a reduced set $\hat{\mathbf{u}}_i^{(s)}$ of (time-dependent) modal coordinates that are related to fixed-interfaces normal modes. These follow from the eigenvalue problem:

$$\left(\mathbf{K}_{ii}^{(s)} - \omega_{ii,j}^{(s)2}\,\mathbf{M}_{ii}^{(s)}\right)\boldsymbol{\phi}_{ii,j}^{(s)} = \mathbf{0} \qquad \Rightarrow \qquad \boldsymbol{\Phi}_{ii}^{(s)} = \left[\boldsymbol{\phi}_{ii,1}^{(s)} \quad \boldsymbol{\phi}_{ii,2}^{(s)} \quad \cdots \quad \boldsymbol{\phi}_{ii,n^{(s)}}^{(s)}\right], \quad (2)$$

where $\boldsymbol{\Phi}_{ii}^{(s)}$ is a modal matrix, and $n^{(s)}$ is (typically) much smaller than the size of $\mathbf{u}_i^{(s)}$. As the interior DoFs are not uncoupled from those related to the component boundaries, the HCB method makes use of static interface constraint-modes in its procedure, corresponding to columns of $\boldsymbol{\Psi}_{ib}^{(s)} = -\mathbf{K}_{ii}^{(s)-1}\mathbf{K}_{ib}^{(s)}$.

Then, by employing $\mathbf{u}_i^{(s)} \approx \boldsymbol{\Psi}_{ib}^{(s)}\hat{\mathbf{u}}_b^{(s)} + \boldsymbol{\Phi}_{ii}^{(s)}\hat{\mathbf{u}}_i^{(s)}$, being $\hat{\mathbf{u}}_b^{(s)} \equiv \mathbf{u}_b^{(s)}$, the partially reduced EoMs of a substructure s are given by:

$$\begin{bmatrix} \widehat{\mathbf{M}}_{bb}^{(s)} & \widehat{\mathbf{M}}_{bi}^{(s)} \\ \widehat{\mathbf{M}}_{ib}^{(s)} & \mathbf{I} \end{bmatrix} \begin{Bmatrix} \ddot{\hat{\mathbf{u}}}_b^{(s)} \\ \ddot{\hat{\mathbf{u}}}_i^{(s)} \end{Bmatrix} + \begin{bmatrix} \widehat{\mathbf{K}}_{bb}^{(s)} & \mathbf{0} \\ \mathbf{0} & \boldsymbol{\Lambda}^{(s)} \end{bmatrix} \begin{Bmatrix} \hat{\mathbf{u}}_b^{(s)} \\ \hat{\mathbf{u}}_i^{(s)} \end{Bmatrix} = \begin{Bmatrix} \hat{\mathbf{f}}_b^{(s)} \\ \hat{\mathbf{f}}_i^{(s)} \end{Bmatrix} = \begin{Bmatrix} \mathbf{f}_b^{(s)} \\ \boldsymbol{\Phi}_{ii}^{(s)\mathsf{T}}\mathbf{f}_i^{(s)} \end{Bmatrix} \qquad \Leftrightarrow \qquad \widehat{\mathbf{M}}^{(s)}\ddot{\hat{\mathbf{u}}}^{(s)} + \widehat{\mathbf{K}}^{(s)}\hat{\mathbf{u}}^{(s)} = \hat{\mathbf{f}}^{(s)}, \quad (3)$$

where eigenvectors grouped in $\boldsymbol{\Phi}_{ii}^{(s)}$ satisfy $\boldsymbol{\Phi}_{ii}^{(s)\mathsf{T}}\mathbf{M}_{ii}^{(s)}\boldsymbol{\Phi}_{ii}^{(s)} = \mathbf{I}$, with $\boldsymbol{\Lambda}^{(s)}$ being a diagonal spectral matrix.

Whilst the HCB procedure can enable significant reduction of DoFs pertaining to individual substructures, several boundary DoFs might persist at system-level, i.e., related to an assembly of various substructures. Numerous boundary DoFs might slow down or impede numerical computations, which constitutes a reason for research having been made concerning their reduction. This is the focus of the following subsection.

2.2 Techniques for reducing boundary DoFs

Several procedures have already been devised for the reduction of boundary DoFs after application of the HCB method, as discussed in Section 1. As one cannot delve into too many details inhere, the interested reader can refer to the work by Krattiger *et al.* (2019) or Allen *et al.* (2020) for additional information concerning the matter.

2.2.1 System-level characteristic constraint method

One of the procedures available for the reduction of boundary DoFs makes use of S-CC modes. Basically, inertia and stiffness matrices related to the substructures making the complete system are globally assembled, initially. If boundary DoFs shared by components are all compatible (i.e., they are related to nodes that are coincident, and which share the same DoFs that need to be coupled), then simple linear transformation matrices $\mathbf{L}^{(s)}$ that provide the component DoFs $\hat{\mathbf{u}}^{(s)}$ in terms of global ones, $\hat{\mathbf{u}}^{(g)}$, through $\hat{\mathbf{u}}^{(s)} = \mathbf{L}^{(s)}\hat{\mathbf{u}}^{(g)}$, can be used to obtain:

$$\widehat{\mathbf{M}}^{(g)} = \sum_{s=1}^{N_s} \mathbf{L}^{(s)\mathsf{T}}\widehat{\mathbf{M}}^{(s)}\mathbf{L}^{(s)}, \qquad \widehat{\mathbf{K}}^{(g)} = \sum_{s=1}^{N_s} \mathbf{L}^{(s)\mathsf{T}}\widehat{\mathbf{K}}^{(s)}\mathbf{L}^{(s)}, \qquad \hat{\mathbf{f}}^{(g)} = \sum_{s=1}^{N_s} \mathbf{L}^{(s)\mathsf{T}}\hat{\mathbf{f}}^{(s)}, \quad (4)$$

where N_s is the number of substructures of the system. Alternative procedures based on the Lagrange multiplier technique can be similarly considered, as well (Allen *et al.*, 2020). Irrespective of this choice, S-CC modes are obtained from:

$$\left(\widehat{\mathbf{K}}_{bb}^{(g)} - \widehat{\omega}_{bb,j}^{(g)2}\,\widehat{\mathbf{M}}_{bb}^{(g)}\right)\widehat{\boldsymbol{\phi}}_{bb,j}^{\text{S-CC}} = \mathbf{0} \qquad \Rightarrow \qquad \widehat{\boldsymbol{\Phi}}_{bb}^{\text{S-CC}} = \left[\widehat{\boldsymbol{\phi}}_{bb,1}^{\text{S-CC}} \quad \widehat{\boldsymbol{\phi}}_{bb,2}^{\text{S-CC}} \quad \cdots \quad \widehat{\boldsymbol{\phi}}_{bb,n^{\text{S-CC}}}^{\text{S-CC}}\right], \quad (5)$$

where $\mathbf{A}_{bb}^{(g)}$, for $\mathbf{A} = \mathbf{M}, \mathbf{K}$, indicates the partition of a global matrix which is related to boundary DoFs, yet to be reduced. This is accomplished using $\hat{\mathbf{u}}_b^{(g)} = \widehat{\boldsymbol{\Phi}}_{bb}^{\text{S-CC}}\tilde{\mathbf{u}}_b^{(g)}$, with $n^{\text{S-CC}}$ corresponding to the number of S-CC modes used to approximate the response of the physical boundary DoFs $\hat{\mathbf{u}}_b^{(g)}$ into generalized coordinates $\tilde{\mathbf{u}}_b^{(g)}$.

Based on such exposition, and considering that $\tilde{\mathbf{u}}_i^{(g)} \equiv \hat{\mathbf{u}}_i^{(g)}$, the EoMs which result after reduction of boundary DoFs by the S-CC method are given by:

$$\begin{bmatrix} \widetilde{\mathbf{M}}_{bb}^{\text{S-CC}} & \widetilde{\mathbf{M}}_{bi}^{\text{S-CC}} \\ \widetilde{\mathbf{M}}_{ib}^{\text{S-CC}} & \mathbf{I} \end{bmatrix} \begin{Bmatrix} \ddot{\tilde{\mathbf{u}}}_b^{(g)} \\ \ddot{\tilde{\mathbf{u}}}_i^{(g)} \end{Bmatrix} + \begin{bmatrix} \widetilde{\mathbf{K}}_{bb}^{\text{S-CC}} & \mathbf{0} \\ \mathbf{0} & \boldsymbol{\Lambda}^{(g)} \end{bmatrix} \begin{Bmatrix} \tilde{\mathbf{u}}_b^{(g)} \\ \tilde{\mathbf{u}}_i^{(g)} \end{Bmatrix} = \begin{Bmatrix} \tilde{\mathbf{f}}_b^{(g)} \\ \tilde{\mathbf{f}}_i^{(g)} \end{Bmatrix} = \begin{Bmatrix} \left(\boldsymbol{\Phi}_{bb}^{\text{S-CC}}\right)^{\mathsf{T}}\hat{\mathbf{f}}_b^{(g)} \\ \hat{\mathbf{f}}_i^{(g)} \end{Bmatrix}. \quad (6)$$

2.2.2 Local-level characteristic constraint methods

While the S-CC method is conceptually simple, and it is usually able to provide reduced-order models that perform well, the eigenvalue problem presented in Eq. (5) can have large size, posing issues for such method. Therefore, alternative strategies focus on reducing boundary DoFs *before* assembling global matrices of the structural system, exploring local-level characteristic constraints (L-CC) modes.

Depending on how L-CC modes are evaluated and grouped to provide reduction bases for boundary DoFs, compatibility equations that must be enforced for assembling components might be satisfied either exactly or approximately. This gives rise to L-CC methods featuring "exact" or "weak" compatibility, respectively (Krattiger *et al.*, 2019; Allen *et al.*, 2020). Here one considers that compatibility equations are linear on boundary DoFs.

In the EC L-CC method, the reduction basis is constructed as detailed next. First, the following eigenvalue problems are solved, for all substructures:

$$\left(\widehat{\mathbf{K}}_{bb}^{(s)} - \widehat{\omega}_{bb,j}^{(s)2}\,\widehat{\mathbf{M}}_{bb}^{(s)}\right)\widehat{\boldsymbol{\phi}}_{bb,j}^{(s)\text{L-CC}} = \mathbf{0} \qquad \Rightarrow \qquad \widehat{\boldsymbol{\Phi}}_{bb}^{(s)\text{L-CC}} = \left[\widehat{\boldsymbol{\phi}}_{bb,1}^{(s)\text{L-CC}} \quad \widehat{\boldsymbol{\phi}}_{bb,2}^{(s)\text{L-CC}} \quad \cdots \quad \widehat{\boldsymbol{\phi}}_{bb,n^{(s)\text{L-CC}}}^{(s)\text{L-CC}}\right]. \tag{7}$$

Then, the boundary DoFs of substructure s can be related to multiple interfaces $\Gamma_i^{(g)}$, on account of the b partition of substructure s collecting all its boundary DoFs, irrespective of which interfaces they are related with. So, in general, one can partition $\widehat{\boldsymbol{\Phi}}_{bb}^{(s)\text{L-CC}}$ as follows:

$$\widehat{\boldsymbol{\Phi}}_{bb}^{(s)\text{L-CC}} = \left[\left(\widehat{\boldsymbol{\Phi}}_{bb,\,\Gamma_1^{(s)}}^{(s)\text{L-CC}}\right)^{\mathsf{T}} \quad \left(\widehat{\boldsymbol{\Phi}}_{bb,\,\Gamma_2^{(s)}}^{(s)\text{L-CC}}\right)^{\mathsf{T}} \quad \cdots \quad \left(\widehat{\boldsymbol{\Phi}}_{bb,\,\Gamma_{\mathsf{n}_s}^{(s)}}^{(s)\text{L-CC}}\right)^{\mathsf{T}}\right]^{\mathsf{T}}, \tag{8}$$

considering how boundary DoFs are distributed along the n_s interfaces $\Gamma_1^{(s)}, \ldots, \Gamma_{\mathsf{n}_s}^{(s)}$ shared by substructure s. Clearly, each $\Gamma_j^{(s)}, j = 1, \ldots, \mathsf{n}_s$, must coincide with one, and only one, $\Gamma_i^{(g)}$. Then, for each interface $\Gamma_i^{(g)}$, one can concatenate L-CC modes pertaining to the various components related to it, i.e.:

$$\widehat{\boldsymbol{\Phi}}_{bb,\,\Gamma_i^{(g)}}^{\text{L-CC}} = \left[\widehat{\boldsymbol{\Phi}}_{bb,\,\Gamma_i^{(g)}}^{(s_1^{(i)})\text{L-CC}} \quad \cdots \quad \widehat{\boldsymbol{\Phi}}_{bb,\,\Gamma_i^{(g)}}^{(s_{\mathsf{n}_i}^{(i)})\text{L-CC}}\right], \tag{9}$$

where $s_j^{(i)}, j = 1, \ldots, \mathsf{n}_i$, indicate substructures, the boundaries of which share at least some DoFs with interface $\Gamma_i^{(g)}$, n_i being the total amount of such substructures. Equation (9) might lead to ill conditioning issues, as eigenvectors being grouped not necessarily are linearly independent. To avoid any risk, one can resort to singular value decomposition (SVD) to obtain a new set of orthogonal vectors spanning the same column space of $\widehat{\boldsymbol{\Phi}}_{bb,\,\Gamma_i^{(g)}}^{\text{L-CC}}$:

$$\widehat{\boldsymbol{\Phi}}_{bb,\,\Gamma_i^{(g)}}^{\text{L-CC}} = \mathbf{U}_{bb,\,\Gamma_i^{(g)}}^{\text{L-CC}}\,\boldsymbol{\Sigma}_{bb,\,\Gamma_i^{(g)}}^{\text{L-CC}}\left(\mathbf{V}_{bb,\,\Gamma_i^{(g)}}^{\text{L-CC}}\right)^{\mathsf{T}}. \tag{10}$$

The referred set of vectors are collected in the matrix of left singular vectors $\mathbf{U}_{bb,\,\Gamma_i^{(g)}}^{\text{L-CC}}$. Those columns of $\mathbf{U}_{bb,\,\Gamma_i^{(g)}}^{\text{L-CC}}$ that are related to singular values smaller than a specified (relative) threshold σ_R are discarded (Krattiger *et al.*, 2019). The resulting matrices can then be used to reduce all boundary DoFs vectors related to interfaces $\Gamma_i^{(g)}$, independent of which substructure they are related with — a consequence of the concatenation performed in Eq. (9). Accordingly:

$$\hat{\mathbf{u}}_b^{(s_j^{(i)})} = \mathbf{U}_{bb,\,\Gamma_i^{(g)}}^{\text{L-CC}}\,\tilde{\mathbf{u}}_b^{(g,i)}, \quad j = 1, \ldots, \mathsf{n}_i, \tag{11}$$

where i in $\tilde{\mathbf{u}}_b^{(g,i)}$ indicates a partition of the global reduced boundary DoFs related to interface i. These partitions are grouped just like shown afterwards in Eq. (15). Taking $\hat{\mathbf{u}}_b^{(g)}$ as a global set of *independent* boundary DoFs, and noting that $\hat{\mathbf{u}}_{b,\,\Gamma_j^{(s)}}^{(s)}$ corresponds to the partition of $\hat{\mathbf{u}}_b^{(s)}$ related to the interface $\Gamma_j^{(s)}$, it is possible to see that:

$$\hat{\mathbf{u}}_{b,\,\Gamma_j^{(s)}}^{(s)} = \mathbf{B}^{(s_j)}\hat{\mathbf{u}}_b^{(g)}, \tag{12}$$

where $\mathbf{B}^{(s_j)}$ constitutes a Boolean localization matrix. It then follows that:

$$\hat{\mathbf{u}}_b^{(s)} = \left\{\hat{\mathbf{u}}_{b,\,\Gamma_1^{(s)}}^{(s)\mathsf{T}} \quad \hat{\mathbf{u}}_{b,\,\Gamma_2^{(s)}}^{(s)} \quad \cdots \quad \hat{\mathbf{u}}_{b,\,\Gamma_{\mathsf{n}_s}^{(s)}}^{(g)\mathsf{T}}\right\}^{\mathsf{T}} = \mathbf{B}^{(s)}\hat{\mathbf{u}}_b^{(g)} \qquad \text{with} \qquad \mathbf{B}^{(s)} = \text{blkdiag}\left(\mathbf{B}^{(s_1)}, \mathbf{B}^{(s_2)}, \ldots, \mathbf{B}^{(s_{\mathsf{n}_s})}\right). \tag{13}$$

Now, due the reduction of boundary DoFs, it also follows that:

$$\hat{\mathbf{u}}_b^{(g)} = \mathbf{U}_{bb}^{\text{L-CC}}\tilde{\mathbf{u}}_b^{(g)}, \qquad \text{where} \qquad \mathbf{U}_{bb}^{\text{L-CC}} = \text{blkdiag}\left(\mathbf{U}_{bb,\,\Gamma_1^{(g)}}^{\text{L-CC}}, \mathbf{U}_{bb,\,\Gamma_2^{(g)}}^{\text{L-CC}}, \ldots, \mathbf{U}_{bb,\,\Gamma_{N_i}^{(g)}}^{\text{L-CC}}\right), \tag{14}$$

and $\tilde{\mathbf{u}}_b^{(g)}$ representing the vector of modal DoFs related to the L-CC modes, which can be partitioned as:

$$\tilde{\mathbf{u}}_b^{(g)} = \left\{ \tilde{\mathbf{u}}_b^{(g,1)\mathsf{T}} \quad \tilde{\mathbf{u}}_b^{(g,2)\mathsf{T}} \quad \cdots \quad \tilde{\mathbf{u}}_b^{(g,N_i)\mathsf{T}} \right\}^{\mathsf{T}}. \tag{15}$$

By combining Eqs. (13) and (14), one can further write:

$$\hat{\mathbf{u}}_b^{(s)} = \mathbf{B}^{(s)} \hat{\mathbf{u}}_b^{(g)} = \mathbf{B}^{(s)} \mathbf{U}_{bb}^{\text{L-CC}} \tilde{\mathbf{u}}_b^{(g)} = \mathbf{U}_{bb}^{(s)\text{L-CC}} \tilde{\mathbf{u}}_b^{(g)} \qquad \Leftrightarrow \qquad \mathbf{U}_{bb}^{(s)\text{L-CC}} = \mathbf{B}^{(s)} \mathbf{U}_{bb}^{\text{L-CC}}. \tag{16}$$

Hence, considering the above, the EoMs that result when employing the EC L-CC method to reduce boundary DoFs are given by:

$$\begin{bmatrix} \widetilde{\mathbf{M}}_{bb}^{\text{EC L-CC}} & \widetilde{\mathbf{M}}_{bi}^{\text{EC L-CC}} \\ \widetilde{\mathbf{M}}_{ib}^{\text{EC L-CC}} & \mathbf{I} \end{bmatrix} \begin{Bmatrix} \ddot{\tilde{\mathbf{u}}}_b^{(g)} \\ \ddot{\tilde{\mathbf{u}}}_i^{(g)} \end{Bmatrix} + \begin{bmatrix} \widetilde{\mathbf{K}}_{bb}^{\text{EC L-CC}} & \mathbf{0} \\ \mathbf{0} & \mathbf{\Lambda}^{(g)} \end{bmatrix} \begin{Bmatrix} \tilde{\mathbf{u}}_b^{(g)} \\ \tilde{\mathbf{u}}_i^{(g)} \end{Bmatrix} = \begin{Bmatrix} \tilde{\mathbf{f}}_b^{(g)} \\ \tilde{\mathbf{f}}_i^{(g)} \end{Bmatrix}. \tag{17}$$

Similar reduced-order EoMs can be written when the WC L-CC method is used to reduce boundary DoFs. As explained by Krattiger *et al.* (2019), when L-CC modes are not concatenated to form Eq. (9), which guarantees exact compatibility for coupling substructures into an assembly, compatibility at the substructure interfaces must be enforced approximately. Linear combination of interface modes that approximately satisfies compatibility between substructures must therefore be defined, which requires the specification of a given tolerance. This tolerance value significantly affects the performance of interface reduction. Its value cannot be determined straightforwardly, and an optimal value that balances interface mode truncation error and inexact compatibility error should be pursued by numerical experimentation, which is not always suitable.

2.2.3 Alternative L-CC method exploring component-level global modes

An aspect which one believes can be improved in the L-CC MOR approach presented in Section 2.2.2 has relation with the eigenvalue problem seen in Eq. (7). As can be clearly understood, it comprises the boundary DoFs of each substructure separately. Thus, it completely disregards the coupling that exists between the boundary and interior DoFs of a substructure. This negligence does not aid the reduction process, and may cause the MOR technique to require an excessive amount of L-CC modes for accurate results to be obtained.

Accordingly, a novel strategy for interface reduction that considers the substructure(component)-level global eigenvalue problem is proposed, inspired by work done on periodic structures (Santos *et al.*, 2025):

$$\left(\widehat{\mathbf{K}}^{(s)} - \widehat{\omega}_j^{(s)2} \, \widehat{\mathbf{M}}^{(s)} \right) \widehat{\boldsymbol{\phi}}_j^{(s)\text{GS L-CC}} = \mathbf{0}, \tag{18}$$

where eigenvectors $\widehat{\boldsymbol{\phi}}_j^{(s)\text{GS L-CC}}$ are determined considering the coupled behavior between (modal) interior and (physical) boundary DoFs of each substructure. Within this framework, one extracts the boundary DoFs partition of $\widehat{\boldsymbol{\phi}}_j^{(s)\text{GS L-CC}}$, $j = 1, \ldots, n_{\text{GS L-CC}}$, and, using them, perform MOR following the same procedures outlined previously in Section 2.2.2, from Eq. (7), essentially.

Whilst this procedure can seem counter-intuitive, as the size of the eigenvalue problem stated in Eq. (18) is larger than the one considered by the EC L-CC method, the proposed "global-substructure" EC L-CC (GS EC L-CC) technique is expected to be more accurate than other state-of-the-art methods because it takes into account the coupled dynamic behavior between the boundary and interior DoFs of a substructure, an outcome that has been observed in the MOR of boundary DoFs of unit cells in periodic-like structures. Authors believe this can be most relevant when i) couplings between substructures do not involve only line–line interfaces, i.e., they are related to potentially non-planar surfaces, for example; and/or ii) interfaces have more or less the same dynamic stiffness relative to interior subdomains, such that the interaction between interior and boundary DoFs shows itself more relevant.

It should be highlighted that a Modal Assurance Criterion (MAC) strategy can be employed to eliminate redundant modes in the GS EC L-CC projection matrices (Santos *et al.*, 2025). Basically, the auto-MAC is computed for the eigenvector matrices used in the reduction of the substructure interfaces. Highly similar eigenvectors are then identified and discarded based on a threshold value defined for the filtering strategy. The procedure consists of comparing each eigenvector of individual modal matrices (related to a particular interface) with the remaining eigenvectors included in the same basis. Eigenvectors exhibiting high correlation, say with a MAC index greater than 0.8, can be eliminated, retaining only one vector from each highly correlated eigenvector group, thereby yielding reduced-order models of smaller size and enhanced numerical stability.

Although boundary DoFs of substructures are reduced in a manner very similar to that described in Section 2.2.2 within the GS EC L-CC framework, eigenvectors are orthogonalized differently. In the novel L-CC MOR method, Eq. (9) is orthogonalized to avoid ill-conditioning issues. This procedure is again performed using SVD; however, in this case, it is implemented directly through the MATLAB® command `orth` (MATLAB, 2025). Usually, few, if any, eigenvectors are eliminated in this step, contrary to what has been discussed in Section 2.2.2, because i) the MAC-based mode removal

strategy already eliminates nearly collinear modes from eigenvector matrices, and ii) threshold values used by MATLAB® to truncate eigenvectors are typically very tight/small (by default, they are computed as `max(size(`$\boldsymbol{\Phi}$`))*eps(norm(`$\boldsymbol{\Phi}$`))`, where `max`, `size`, `eps`, and `norm` are native MATLAB® functions, and $\boldsymbol{\Phi}$ denotes the eigenvector matrix being orthogonalized). In this context, orthgonalization is therefore employed solely to avoid singularity issues that may arise during MOR if eigenvectors are not orthogonalized (Krattiger *et al.*, 2019).

3. NUMERICAL EXPERIMENTS

The system analyzed in this work has been presented previously, see Fig. 1. Table 1 provides additional data that have been used to perform simulations. In particular, one has focused on modal and forced harmonic analyses. Free-free boundary conditions were considered. The external force used to excite the structural assembly was taken to be applied at the node at $x = 304.8\,\text{mm}$, $y = 0\,\text{mm}$, $z = 203.2\,\text{mm}$, being it directed along the y axis (cf. Fig. 6 to be discussed later), to induce bending on substructure 3.

Table 1: Data used to perform numerical experiments.

Method	Max. frequency (Hz)	Threshold multiplier	Truncation freq. (Hz)
HCB	1000	1.8 (Géradin, 2015)	1800
S-CC / EC L-CC / WC L-CC / GS EC L-CC	1000	1.2 (Santos *et al.*, 2025)	1200

The material of all plates is assumed as 2024-T3 Aluminum, with density $\rho = 2800\,\text{kg}\,\text{m}^{-3}$, Young's modulus $E = 72\,\text{GPa}$, and Poisson's ratio $\nu = 0.33$. The thickness of all plates was taken equal to $0.125\,\text{in} = 3.175\,\text{mm}$.

First, interior DoFs of each substructure of the W-bracket system presented in Fig. 1 were reduced using the HCB method. Table 2 shows the number of physical and modal DoFs of each substructure. The numbers of physical DoFs and fixed-interface modes for substructures 3, 4, and 5 are identical, since these components have equal geometry and material properties. Therefore, 2400 interior DoFs were reduced to 14 for each of these substructures. On the other hand, the number of physical interior DoFs was reduced from 4650 and 2250 to 22 and 9 for substructures 1 and 2, respectively. In total, 14100 interior DoFs were reduced to 73 generalized coordinates using the HCB method.

Table 2: Number of physical and modal interior DoFs of each substructure.

	Number of interior DoFs of each substructure					
	Substructure 1	Substructure 2	Substructure 3	Substructure 4	Substructure 5	Total
Physical (full model)	4650	2250	2400	2400	2400	14100
Modal (reduced model)	22	9	14	14	14	73

Afterwards, the reduction of interface DoFs is carried out according to the methods summarized in Section 2.2, Table 3 shows the number of physical and modal DoFs for the W-bracket system presented in Fig. 1, as well as relevant data concerning the HCB W-bracket model, which is helpful to evaluate the MOR performance. Fields with no information to be displayed are indicated in Table 3 with dashes (–), whereas a hash symbol (#) is used to indicate that the corresponding quantity cannot be defined or reported due to the formulation adopted in the model reduction procedure.

Table 3: Number of physical and modal DoFs for the W-bracket model.

		Number of interior and boundary DoFs				
		Method				
		HCB	S-CC	EC L-CC	GS EC L-CC	WC L-CC
Physical (full model)	Interior	14100	14100	14100	14100	14100
	Interfaces	450	450	450	450	450
	Total	14550	14550	14550	14550	14550
Modal (reduced model)	Interior	73	73	73	73	73
	Interface 1	–	#	19	42	#
	Interface 2	–	#	22	58	#
	Interface 3	–	#	18	32	#
	Total	–	73 + 18 = 91	73 + 59 = 132	73 + 132 = 205	73 + 12 = 85

Table 3 shows that the number of (modal) interface DoFs can vary significantly from one method to another. It ranges from 12 when the WC L-CC MOR formulation is employed to 132 with the novel GS EC L-CC strategy. This occurs because distinct eigenproblems are solved in each interface model reduction strategy, thereby yielding substantially different eigenvalues. As a matter of fact, eigenvectors can also differ considerably, exhibiting dynamic behavior characterized by

either global or local deflections (Krattiger *et al.*, 2019). As discussed previously in Section 2.2.3, the MAC-based strategy can be used to eliminate redundant modes in the GS EC L-CC method by specifying a threshold value for the filtering procedure. In this work, this value has been taken as one (meaning that no redundant mode has been removed), although it could have been adjusted to smaller values. Accordingly, Table 3 indicates that the interface DoFs can be reduced from 450 to 18, 59, 132, or 12 with the S-CC, EC L-CC, GS EC L-CC, or WC L-CC methods, respectively, when frequency truncation is done in accordance with Table 1. In total, the number of physical DoFs of the W-bracket system can be reduced from 14550 to a minimum of 85 (WC-LCC) or a maximum of 205 (GS EC L-CC). This considerable variation in the total amount of modal DoFs of the W-bracket assembly can affect the accuracy of the derived reduced-order models, as investigated next.

Figure 2 shows the comparison of natural frequencies computed using the reference HCB, S-CC, EC L-CC, GS EC L-CC, and WC L-CC reduced-order models. As discussed previously, the reduction of interface DoFs using either of the considered methods was applied to the same HCB-reduced order model. Hence, the gray curve in Fig. 2 (—●—), which is hidden beneath other plots, is admitted as the reference solution. Figure 2 clearly shows that the W-bracket assembly exhibits six zero-frequency modes corresponding to rigid body modes, consistent with the adopted finite element model and free–free boundary conditions. Beyond the sixtieth mode, natural frequencies associated with the flexible-body modes appear to closely match, except for the WC L-CC method, for which the reduced model tends to be stiffer than the reference HCB model and the other models, again, considering the frequency truncation stated in Table 1.

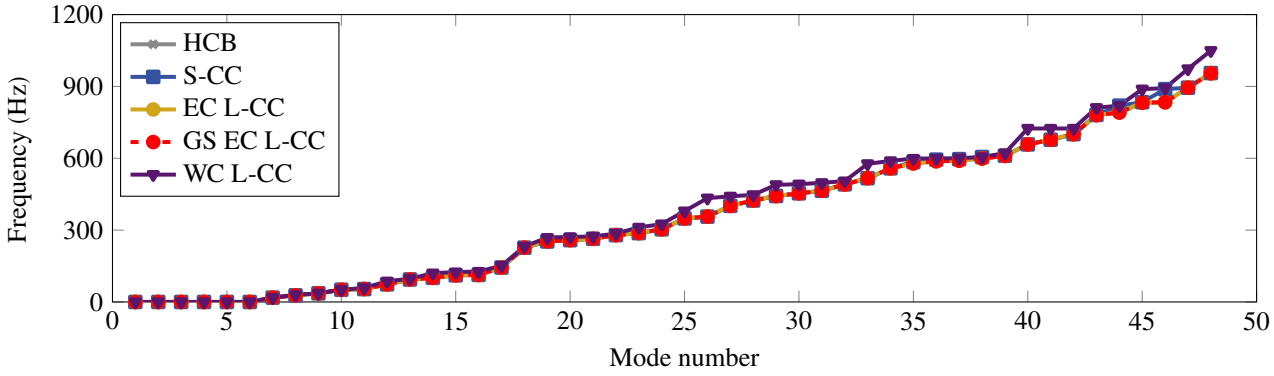


Figure 2: Comparison of natural frequencies computed using the HCB, S-CC, EC L-CC, GS EC L-CC, and WC L-CC reduced-order models, employing frequency truncation as stated in Table 1.

Simulation times for the calculation of the natural frequencies presented in Fig. 2 are summarized in Fig. 3. Simulations were performed on a DELL Precision 7680 laptop equipped with an Intel(R) Core(TM) i9-13950HX (13th generation) processor and 64.0 GB of RAM. As one may observe, the computation of the natural frequencies using the HCB model required the largest simulation time, whereas the other models, which feature the reduction of interface DoFs, show a significant decrease in computational cost. In particular, the WC L-CC and S-CC approaches resulted in the lowest simulation times, followed by the EC L-CC method. The GS EC L-CC approach required a larger computational time than the other interface reduction strategies, although it is still considerably smaller than that required by the HCB model, due to the larger number of equations involved in the associated eigenvalue problem.

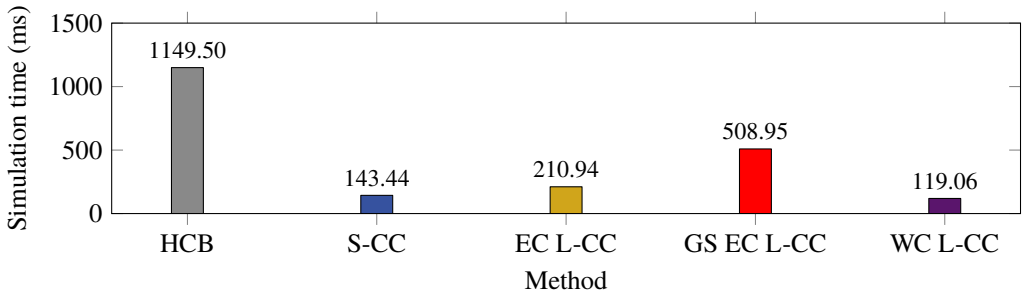


Figure 3: Simulation times required to compute natural frequencies using the HCB, S-CC, EC L-CC, GS EC L-CC, and WC L-CC reduced-order models through the solution of eigenvalue problems.

To investigate the discrepancies between the natural frequencies in Fig. 2, Fig. 4 shows the relative error between them, adopting as reference those obtained with the HCB-reduced model. Results in Fig. 4 reveal that the S-CC interface reduction method outperforms the other strategies for the first low-order modes. As the corresponding natural frequency increases, the accuracy of results computed using S-CC tends to decrease, becoming worse than those obtained with the EC L-CC or

GS EC L-CC strategies. The interface reduction methods based on exact compatibility show similar frequency error for all modes. In fact, the proposed GS EC L-CC interface reduction method performs consistently better than the EC L-CC, in Fig. 4. Lastly, the WC L-CC approach exhibits the worst performance among the considered methods, with frequency errors mostly superior to 1%, reaching more than 20%. This occurs mainly because i) exact compatibility is not enforced at the substructure interfaces, which leads to incorrect couplings when assembling the W-bracket model, and ii) frequency-based truncation criterion appears to be misleading for the WC L-CC interface reduction method, which truncates the eigenvectors at the substructure level (Krattiger *et al.*, 2019) — a problem that has not been observed in the EC-LCC or GS EC-LCC methods. In reality, if the threshold multiplier is updated from 1.2 to 30 for the WC L-CC interface reduction method, then it provides frequency errors similar to those of the EC-LCC, but consistently worst than them (results of which are omitted here). This, however, comes at the cost of increasing the number of (modal) interface modes from 12 (cf. Table 3) to 67.

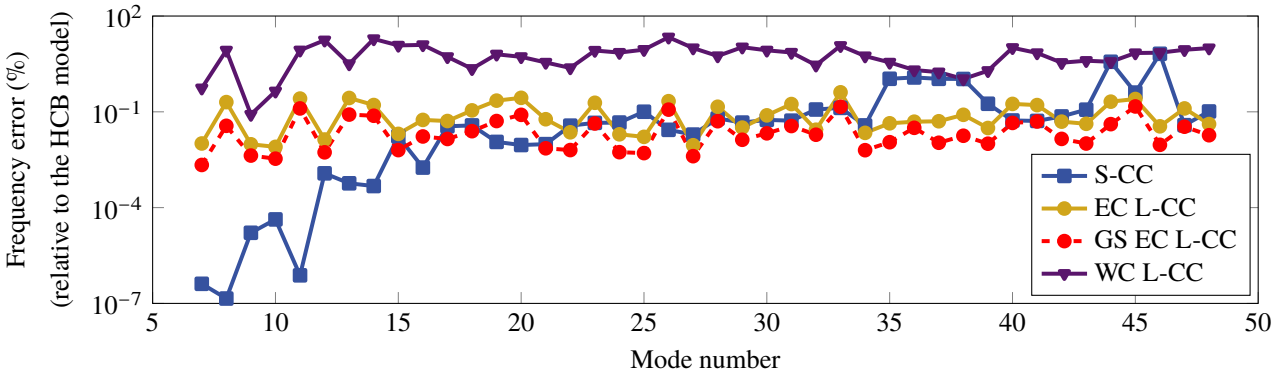


Figure 4: Frequency error of S-CC, EC L-CC, GS EC L-CC, and WC L-CC interface reduction methods relative to the HCB model, considering frequency truncation as specified in Table 1.

Beyond the frequency errors provided in Fig. 4, mode (eigenvector) error also deserves investigation, as mode shapes are often of interest when performing dynamic analyses. The mode error can be defined as 1 minus the MAC index, the latter being computed between eigenvectors obtained using the various interface reduction methods, and the corresponding ones derived with the HCB-reduced model. It is shown for the S-CC, EC L-CC, GS EC L-CC, and WC L-CC interface reduction methods in Fig. 5. As can be noticed, the mode errors follow similar tendencies exhibited by frequency errors in Fig. 4, showing that one is clearly related to the other. In particular, the S-CC interface reduction method exhibits the smallest errors for the lowest order modes, whereas its accuracy deteriorates as the corresponding natural frequency increases. The EC L-CC and GS EC L-CC strategies provide similar results over the considered mode range, with the GS EC L-CC method performing slightly better overall. As to the WC L-CC approach, it yields the poorest agreement with the reference HCB model in general, with several eigenvector pairs showing mode error equal to 100%, again, due to the frequency truncation reported in Table 1.

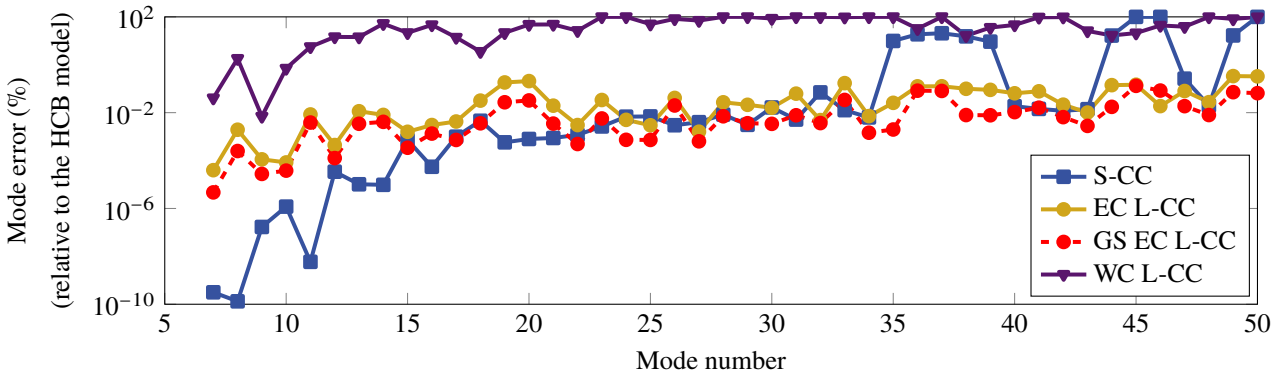


Figure 5: Mode error of S-CC, EC L-CC, GS EC L-CC, and WC L-CC interface reduction methods relative to the HCB model considering the frequency truncation reported in Table 1.

After investigating the frequency and mode errors, there remains the need to analyze forced harmonic results using the considered reduced-order models. Accordingly, Fig. 6 shows frequency response functions (FRFs) computed for the W-bracket structure considering the external force is applied as indicated by the red arrow, and the accelerance response is evaluated at the same node, as indicated by the green arrow, both in accordance with coordinates provided at the beginning of this section. In accordance with previous analyses, the FRF obtained considering the S-CC interface reduction approach is more accurate for smaller frequencies, becoming less accurate at some frequency bands above 500 Hz, where the blue

curve (——) deviates from the reference result (——), the latter being almost indistinguishable from those computed with the EC L-CC and GS EC-LCC techniques (—— and - - - curves). The FRF computed using the WC L-CC interface reduction strategy showed the worst accuracy among the other methods, with many resonance frequencies missing in the response of the W-bracket system (cf. ——), which can be attributed to the adopted truncation threshold. Therefore, to ensure accurate responses are obtained over the widest frequency spectrum, the EC L-CC and GS EC L-CC methods appear to be the most suitable interface reduction strategies, given modes get truncated as specified in Table 1.

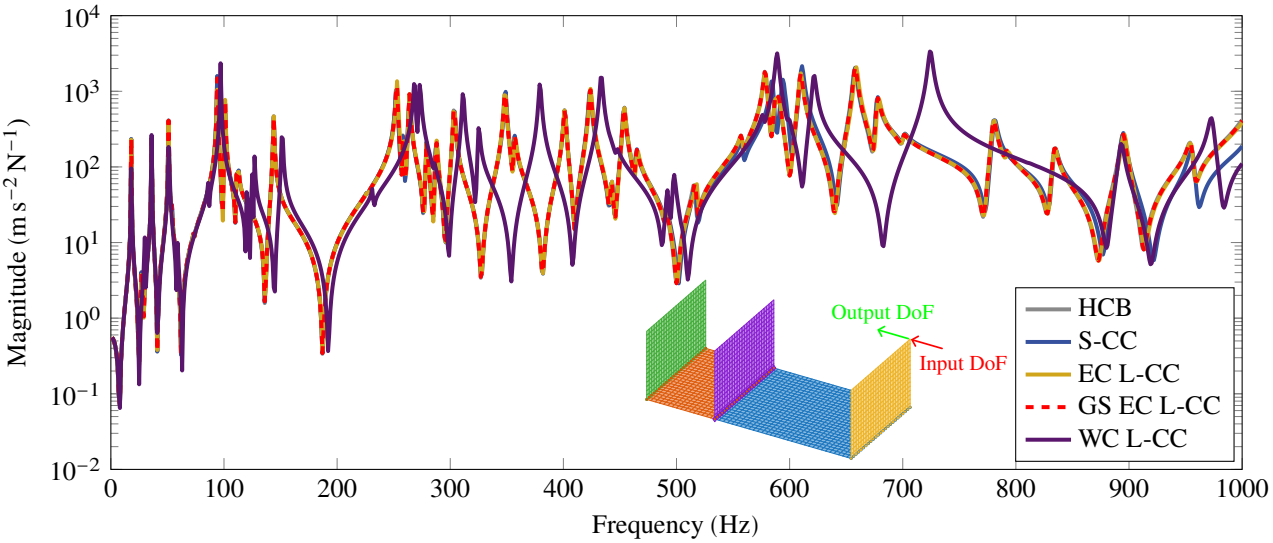
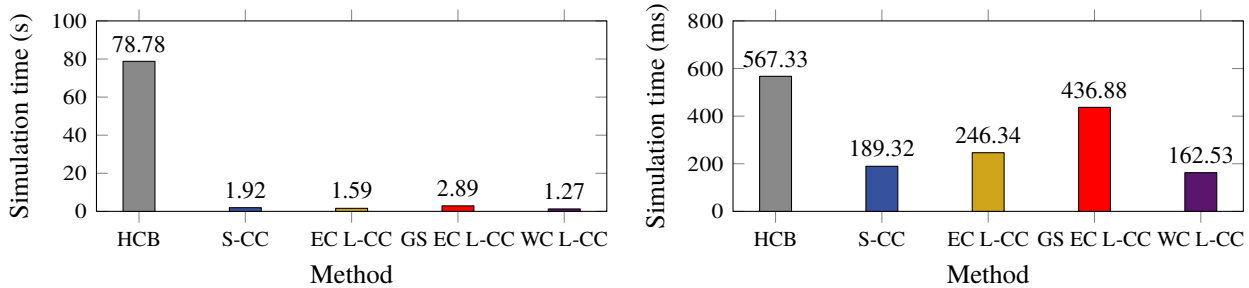


Figure 6: Frequency response functions computed for the W-bracket structure using the HCB, S-CC, EC L-CC, GS EC L-CC, and WC L-CC reduced-order models considering frequency truncation as specified in Table 1.

Lastly, Fig. 7 summarizes the simulation times required to compute the FRFs shown in Fig. 6 by the direct and the modal superposition methods. For the latter, all modes were used; still, computational benefits emerge due to diagonalization. This strategy might not be suitable to more complex systems. Figure 7a clearly shows that computing an FRF by the direct method using the HCB model is much slower than performing the same task using either the S-CC, EC L-CC, GS EC L-CC, or WC L-CC models. Therefore, the reduction of interface DoFs significantly speed up the harmonic analysis of the W-bracket system. On the hand, Fig. 7b shows comparable simulation times irrespective of which reduced-order model is employed for the computation of FRFs by the modal superposition method. In both cases, the proposed GS EC L-CC method showed the highest computational burden among the interface reduction strategies, because it involves manipulating the model with the largest number of equations (cf. Table 3).



(a) (b)

Figure 7: Simulation times required to compute FRFs using the HCB, S-CC, EC L-CC, GS EC L-CC, and WC L-CC reduced-order models by the a) direct method and b) modal superposition method.

4. CONCLUDING REMARKS

This work presented a novel strategy for interface model reduction exploring component-level global modes for substructuring applications. Reduced-order models for substructures were first derived through the well known HCB method, for which interface DoFs remain preserved as physical (unreduced) coordinates. Within the proposed formulation, called GS EC L-CC, the reduction of interface DoFs of substructures has been pursued by solving a component-level global eigenvalue problem, which takes into account the coupling between the substructures boundaries/interfaces and their

interior, independently. Numerical simulations performed on a W-bracket structure composed of five substructures showed that the GS EC L-CC interface reduction method outperformed other interface reduction strategies currently reported in the literature. Forced harmonic analyses demonstrated that the GS EC L-CC method provides good accuracy over a broader frequency range, matching the reference result. Reduced-order models derived employing the proposed interface reduction strategy, however, exhibited a larger number of DoFs compared to competing methods, which could have been mitigated by adjusting the threshold value adopted for filtering redundant modes in the MAC-based strategy. This work therefore introduced a new strategy for dynamic analyses of assembled structures. Future studies will involve the computation of a broader set of forced responses, taking into account different input and output directions; the assessment of the assembly response not only at the interior nodes, but also at the substructure interfaces; and the investigation of other cases showing more intricate couplings between substructures. As a last note, one should highlight that the accuracy of the investigated methods can be improved by considering residual modes in the reductions.

5. ACKNOWLEDGMENTS

This study was financed, in part, by the São Paulo Research Foundation (FAPESP), Brasil. Process Numbers #2018/15894-0, #2023/11207-7 and #2024/07549-2. All authors are grateful to FAPESP for the provided grants. V. M. S. Santos and T. P. Sales also acknowledge the Brazilian Coordination for the Improvement of Higher Education Personnel (CAPES). M. Ouisse acknowledges the graduate school EIPHI (project ANR-17-EURE-0002).

6. REFERENCES

Allen, M.S., Rixen, D., van der Seijs, M., Tiso, P., Abrahamsson, T. and Mayes, R.L., 2020. *Substructuring in Engineering Dynamics: Emerging Numerical and Experimental Techniques*. Springer. doi:10.1007/978-3-030-25532-9.

Aoyama, Y. and Yagawa, G., 2001. "Component mode synthesis for large-scale structural eigenanalysis". *Comput. Struct.*, Vol. 79, No. 6, pp. 605–615. doi:10.1016/s0045-7949(00)00165-6.

Castanier, M.P., Tan, Y.C. and Pierre, C., 2001. "Characteristic constraint modes for component mode synthesis". *AIAA J.*, Vol. 39, No. 6, pp. 1182–1187. doi:10.2514/2.1433.

Craig, R.R. and Bampton, M.C.C., 1968. "Coupling of substructures for dynamic analyses". *AIAA J.*, Vol. 6, No. 7, pp. 1313–1319. doi:10.2514/3.4741.

Craig, R.R. and Kurdila, A., 2006. *Fundamentals of structural dynamics*. John Wiley & Sons, 2nd edition.

Donders, S., Pluymers, B., Ragnarsson, P., Hadjit, R. and Desmet, W., 2010. "The wave-based substructuring approach for the efficient description of interface dynamics in substructuring". *J. Sound Vib.*, Vol. 329, No. 8, pp. 1062–1080. doi:10.1016/j.jsv.2009.10.022.

Géradin, M., 2015. *Mechanical Vibrations: Theory and Application to Structural Dynamics*. John Wiley & Sons, 3rd edition.

Hong, S.K., Epureanu, B.I. and Castanier, M.P., 2013. "Next-generation parametric reduced-order models". *Mech. Syst. Signal Pr.*, Vol. 37, No. 1–2, pp. 403–421. doi:10.1016/j.ymssp.2012.12.012.

Krattiger, D., Wu, L., Zacharczuk, M., Buck, M., Kuether, R.J., Allen, M.S., Tiso, P. and Brake, M.R.W., 2019. "Interface reduction for Hurty/Craig-Bampton substructured models: Review and improvements". *Mech. Syst. Signal Pr.*, Vol. 114, pp. 579–603. doi:10.1016/j.ymssp.2018.05.031.

Kuether, R.J., Allen, M.S. and Hollkamp, J.J., 2017. "Modal substructuring of geometrically nonlinear finite element models with interface reduction". *AIAA J.*, Vol. 55, No. 5, pp. 1695–1706. doi:10.2514/1.j055215.

Lindberg, E., Hörlin, N.E. and Göransson, P., 2013. "Component Mode Synthesis Using Undeformed Interface Coupling Modes to Connect Soft and Stiff Substructures". *Shock Vib.*, Vol. 20, No. 1, pp. 157–170. doi:10.1155/2013/262354.

MATLAB, 2025. *version 25.2.0.3123386 (R2025b) Update 3. The MathWorks Inc. orth*. [Accessed 4 March 2026]. URL `https://www.mathworks.com/help/matlab/ref/orth.html`.

Santos, V.M.S., Sales, T.P. and Ouisse, M., 2025. "Improving the computation of forced responses of periodic structures by the wave-based finite element method via a modified generalized Bloch mode synthesis". *Finite Elem. Anal. Des.*, Vol. 245, p. 104314. doi:10.1016/j.finel.2025.104314.

Tran, D.M., 2001. "Component mode synthesis methods using interface modes. Application to structures with cyclic symmetry". *Comput. Struct.*, Vol. 79, No. 2, pp. 209–222. doi:10.1016/s0045-7949(00)00121-8.

Tran, D.M., 2009. "Component mode synthesis methods using partial interface modes: Application to tuned and mistuned structures with cyclic symmetry". *Comput. Struct.*, Vol. 87, No. 17–18, pp. 1141–1153. doi:10.1016/j.compstruc.2009.04.009.

Young, J. and Wixom, A., 2026. "Interface reduced substructuring using polynomials for non-smooth line-like interfaces". *J. Sound Vib.*, Vol. 623, p. 119502. doi:10.1016/j.jsv.2025.119502.

7. RESPONSIBILITY NOTICE

The authors are solely responsible for the printed material included in this paper.